Impact of Lanthanum Doping on the Structural, Electrical, and Magnetic Properties of $BaFe_{12}O_{19}$ Nano Particles

Zaheer Abbas Gilani[1], Siraj Ul Islam[1], H. M. Noor ul Huda Khan Asghar[1*], Rafaqat Husssain[1], Furhaj Ahmad Shaikh[1]

[1] Department of Physics, Balochistan University of Information Technology, Engineering & Management Sciences, Quetta 87300, Pakistan

ARTICLE INFO	ABSTRACT
	These ferrites had been considered very highly valuable electronic materials for many decades. The ferrite compounds have a hexagonal structure. Nano structural and dielectric features for $BaFe_{12-x}La_xO_{19}$ (0.00, 0.25.0.50, 0.75, 1.00) nano Hexaferrite (NHFs) was studied present research. The Ba NHF prepared via sol-gel technique. The single phase of barium Nano Hexaferrites of various sample was confirmed by XRD, the average crystalline size calculated in the range of 5 to 13nm. The lattice parameter lattice constant, X-ray density, bulk density, micro strain and lattice strain are the parameters of XRD which are also calculated. The different parameters of XRD also show the decreasing and increasing trend which is totally depend on the concentration. The hexagonal structure also confirmed by FTIR. There are two frequency band are investigated which are $υ_1$ and $υ_2$ which are associated with tetrahedral stretching band and octahedral stretching band respectively. The different frequency band are calculated at different frequency like $υ_1$= 500 to 540 and $υ_2$= 413. The dielectric properties also measured in the frequency range from 1 MHz to 3 GHz. There are many others parameters are calculated in dielectric properties such as real and imaginary electric modulus, real and imaginary impedance, dielectric constant, dielectric loss and tangent loss. The parameters of dielectric also showing decreasing and increasing in trend. The real and imaginary impedance plot changes as when the frequency increases, the all the specimens converge on one another, and at a higher frequency, the impedance exhibits coherent nature, which is due to the discharge of space charges.

*Corresponding Author's Email: noorulhudakhan@gmail.com

1. Introduction

In today's environment, magnetic materials are critical components of technology. Humans have recognized the relevance of ferrites for many years by researching their many characteristics (Smit & Wijn, 1959). The improvement and development of ferrites is mostly dependent on the advancement and development of methods. Different characteristics of ferrites, such as magnetization, electrical conductivity and permittivity, and dielectric losses, can be controlled by chemical composition, annealing, and doped metal ions (Al-Hilli, Li, & Kassim, 2012; Gilani et al., 2015). The magnetic and electrical characteristics of Barium hexa ferrite are the most well-known. Such materials are ideally suited due to their strong electrical resistance capabilities. They are widely used in the manufacture of microwave devices. Because of their wide range of applications, barium Hexaferrites are

important magnetic materials. These materials are synthesized in a variety of ways due to their ease of manufacture, low cost, and high chemical stability (Hussain et al., 2011). Sol-gel technique is used to make these ferrites (Garcia, Bilovol, & Socolovsky, 2012). With the use of a standard doping procedure, the dynamic characteristics of these ferrites may be adjusted to meet the requirements. Doping a suitable element in a certain proportion can have a significant impact on the materials' remarkable characteristics (Smit & Wijn, 1959).

The material's crystal structure determines its different characteristics. The characteristics and crystal structure of ferrites are used to classify them. Different ferrites, such as spinel, garnet, and Hexaferrites, have different structures that range from simple to complicated (Carter & Norton, 2007). The crystal phase of $BaLa_xFe_{12-x}O_{19}$, according to the researchers, is a single M-type hexagonal phase. It is important to understand the material's structure in order to examine its characteristics. It is extremely difficult to examine a material's characteristics without first learning about its crystal structure (Cullity, 1978).

The X-ray diffraction study of the compositions $BaLa_xFe_{12-x}O_{19}$ (x = 0, 0.25, 0.50, 0.75, 1.00) is addressed in detail in this work. In a straightforward manner, the entire method of indexing and computing different relevant structural characteristics is presented. This understanding will allow for a more exact examination of other materials' diffraction patterns. The ferrites behave like an inhomogeneous dielectric material made up of strongly conducting grains separated by an air gap or insulating layers known as grain boundaries. The dielectric constant, tangent loss, AC conductivity, and impedance of ferrite may all be modified by annealing and composition (Sheikh et al., 2019). X-ray diffraction (XRD), Fourier transform infrared spectroscopy (FTIR), and dielectric characteristics analyses are used to analyze the prepared ferrite material.

2. Experimental

The production of different compositions of La doped $BaFe_{12}O_{19}$ was done using the sol-gel auto-combustion process. To make the series of samples with the general formula $BaLa_xFe_{12-x}O_{19}$ (x = 0, 0.25, 0.50, 0.75, 1.00), stoichiometric amounts of analytical grade reagents, such as Barium nitrate (99%), iron (III) nitrate (98%), lanthanum (III) nitrate (99%), and citric acid (99.5%), were weighed using a precise digital balance. These metal nitrates and citric acid (which was used as a fuel) were dissolved separately in de-ionized water, then combined to produce the mixed solution. The magnetic pill (stirrer) was inserted into the solution, and the beaker was set on a hot plate. The solution was stirred, and the hotplate temperature was progressively increased to 150°C. For around 1 hour, the sample was stirred and agitated until the gel was produced. The temperature of the sample was raised to 300 °C as the gel was produced. When the gel was begun to burn, it was heated at this temperature for around 1 hour.

It was let to burn regularly. It took around 1hour for the sample to completely burn. Various gases were emitted from the beaker throughout this time. The final result was a dry powder that was homogeneous. The temperature of the hotplate was progressively reduced once the sample had completely burned. The hotplate was turned off after 10 minutes, and the specimen was allowed to cool in normal temperatures. Despite the fact that the material is now in powder form, this was mixed thoroughly using a pestle and mortar. The sample bottle was filled with fine powder. The samples were all made in the same manner. In a muffle furnace, the samples were placed at 700°C for 3 hours. The samples were pelletized with a 4.5-ton pressure by using hydraulic press. The crystal structure of the produced samples was determined using the diffraction pattern obtained from X-ray diffraction (XRD). The XRD was performed using a panalytical Expert Pro to study the crystal structure and determine various crystalline structural characteristics. The range of values for 2θ was specified to be between 10˚and 80˚. To examine tetrahedral and octahedral stretching bands, FTIR analysis was performed. To study the dielectric characteristics of produced ferrite material, an impedance analyzer was used to conduct a dielectric analysis. Several dielectric characteristics, including as the dielectric constant, dielectric loss, tangent loss, AC conductivity, real and imaginary impedance, and modulus, are computed in the frequency range of 1-MHz to 3-GHz, and their changes are investigated as doping increases.

3.   Result and Discussion
3.1.   XRD Analysis

Sol gel auto combustion is used to make barium hexa ferrites with the general chemical formula $BaLa_xFe_{12-x}O_{19}$ (x = 0.0, 0.25, 0.50, 0.75, and 1.00). Powder XRD is used on the Panalytical Expert Pro to analyse the crystalline structure in detail and detect the crystalline phase formation. Using this information, the first job is to identify the crystal structure of the sample. It's far more difficult to figure out the crystal structure of an unknown substance than it is to figure out the structure of a recognized one. The pattern of diffracted lines in a diffraction pattern reveals the crystal structure, the placements of lines reveal the unit cell, and the intensities of the lines reveal the positions of the atoms (Cullity, 1978). The initial step is to identify this structure, which will provide information on the crystal structure in which the material is found. For this, the $\sin2\theta$ values for all main diffraction lines are computed. These values serve as a foundation for resolving the pattern. If certain diffraction lines appear owing to imperfections in the material or for other reasons, it causes issues and necessitates the use of additional talents. Combining the plane-spacing equation with Bragg's law equation yields a relationship that specifies the Miller indices of a given crystal system. For a hexagonal system, for example, this formula may be expressed as

$$Sin^2\theta = A(h^2+hk+k^2)+Cl^2 \tag{1}$$

In this relation, $A = \lambda^2/3a^2)$ and $C = (\lambda^2/4c^2)$. value of A can be calculated from hkl (l=0). The x - ray diffraction pattern of all concentrations of la^{+3} dopant have been analyzed, all X – ray diffraction values have been observed and shown on the basis of a JCPDS card (reference no 00-027-1029), which shows us a values such as (106), (107) (200) (205) (1110) (300) and (220) at different planes. The values ranged from concentration to concentration, and with the addition of La $^{+3}$, the value of v increases response to the different ionic radii of the la^{+3} and iron. The lattice distortion changed as lanthanum was doped in hexa ferrite. By the substitution of rare earth metal in hexa ferrites the also change were identified in the lattice parameter a and c (Azim, Atiq, Riaz, & Naseem, 2014).
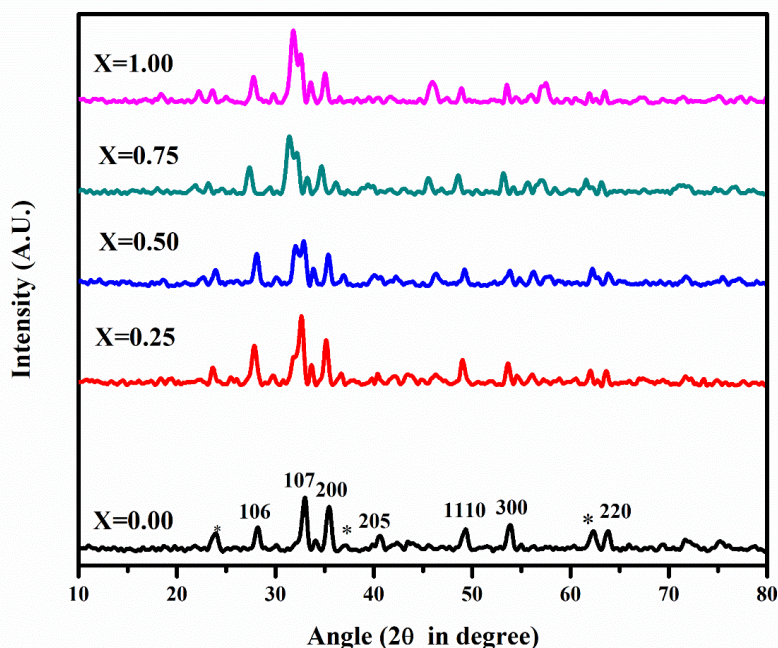
Figure 1: XRD Analysis of BaLa$_x$Fe$_{12-x}$O$_{19}$ (x = 0.0, 0.25, 0.50, 0.75, and 1.00).

The crystalline size is determined using Debye Sherrer's formula for the hkl value of (107)

$$D = k\lambda/\beta\cos\theta \tag{2}$$

From above equation D represent crystal size, λ shows the wavelength which have the value 1.54A°, where k is also another constant which have fixed value 0.89A°, where β shows the full width half maximum. where theta is used for the most intense peaks. The crystal size of the current material doped with rare earth metal ranges from 13.37 nm to 5.84 nm, as shown in table 1, It Tells us about the crystal size in which the trend is regularly decreasing down to 5 nm. The change in curve totally depend on ionic radii of the present material (Fe^{+3}) and the doped materials lanthanum (La^{+3}) (Onreabroy, Papato, Rujijanagul, Pengpat, & Tunkasiri, 2012).

The following formula is used to calculate the lattice constant a and c

$$Sin^2\theta = A\ (h^2 + hk + k^2)\ +\ Cl^2 \tag{3}$$

Where $A = \lambda^2/\ 3\ a^2$ and $C = \lambda^2/\ 4c^2$

First, the standards of the lattice constant "a" range from 5.83 A° to 5.90 A° which are shown in table 1, With different concentrations, it gives different rising and decreasing patterns. The variations are caused by the varying radii of the ions La^{+3} and Fe^{+3}. As a result, the lattice parameter c has also giving a rising and decreasing pattern based on concentration, as shown in table. The ups and downs in the lattice constant trend was caused by the ionic radii of lanthanum and iron, which are in different ranges for "a" and "c" respectively 5.83Å to 5.90Å and 23.1Å to 23.85Å. A particularly fluctuating pattern are because of divergence between ionic radii of accessible and subbed material in fixation.

The following expression was used to calculate the X-ray density.

$$\rho_x = 2M/N_A V \tag{4}$$

Since one-unit cell contains two molecules of the substance, 'M' was its molar concentration of the associated substance, multiplying by '2'. The frequency of Avogadro's number is 6.02×10^{23}, and it is denoted by the letter 'NA.' and the volume of the unit cell is denoted by 'V.' Table values show an improvement in the x-ray density of the relevant hexa ferrite doped with rare earth material, with the cause being an increase in the molecular weight of the substance doped with different amounts. The trend showing the increasing with the concentration level.as we know the molecular weight of iron is 55.84 g/mol and the lanthanum 138.9055 g/mol (Azim et al., 2014; Hussain & Maqsood, 2008).

The bulk density was calculated by the following formula

$$\rho = m/\pi r^2 h \tag{5}$$

Given equation, m indicates mass, r represents the pellet radius in disk shape, h represents the sample's height. The bulk density of all samples have measured, this discovered the rate increases as the lanthanum concentration increases.it also show some decreasing in trend due to ionic radii.

Table 1
Calculated different parameters of XRD of BaLa$_x$Fe$_{12-x}$O$_{19}$ (X= 0.00, 0.25, 0.50, 0.75, 1.00)

Parameters	X=0.00	X=0.25	X=0.50	X=0.75	X=1.00
Crystalline size (nm)	13.379936	12.193954	5.840577	6.1512175	6.3740861
Lattice constant a (Å)	5.839255	5.889154	5.841297	5.90298	5.884243
Lattice constant c (Å)	23.82	23.11	23.28	23.1	23.81
Cell volume	199.10048	204.24843	199.30943	205.69035	203.73788
x-ray density (gc/m^3)	73.494036	76.802935	76.320313	80.182300	80.826302
Bulk density (gc/m^3)	2.1084849	2.501271	2.5638718	2.4333474	2.2706820

Lattice strain was calculated by the following formula which is commonly known as stokes Wilson formula, mathematically this formula is written as

$$Lattice\ strain = \varepsilon = \beta \times cos\theta\ /\ 4tan(\theta)\times 10^{-3} \tag{6}$$

Where ε show the lattice strain and the here β was known as FWHM.

Micro strain was calculated by the following formula, mathematically this formula is written as

$$\text{Micro strain} = \beta \times \cos\theta/4 \times 10^{-3} \tag{7}$$

The following mathematical expression was used to calculate the staking fault of $BaLa_xFe_{12-x}O_{19}$ (X= 0.00, 0.25, 0.50, 0.75, 1.00).

$$\text{Staking fault (SF)} = 2\pi^2/45/ \sqrt{3}\tan(\theta) \tag{8}$$

The dislocation density was calculated by the following mathematical expression

$$\delta = 1/D^2 \times 10^{15} \text{ lines /meter} \tag{9}$$

The Lattice strain, Micro strain, Dislocation density and Staking fault trend increasing and decreasing at different level, which is depend upon the different concentration of rare earth metal lanthanum doped (Azim et al., 2014). The notable values are shown in table 2.

Table 2
Calculated different parameters of XRD of BaLa$_x$Fe$_{12-x}$O$_{19}$ (X=0.00, 0.25, 0.50, 0.75, 1.00)

Parameters	X=0.00	X=0.25	X=0.50	X=0.75	X=1.00
Lattice strain (10^{-3})	8.985351933	10.57688352	20.21259872	21.81314327	21.85618795
Micro strain (10^{-3}) lines^{-4}/meter^{-4}	2.551977734	2.973008241	5.732231212	6.114914363	6.154438432
Dislocation density 10^{15} lines /meter	5.546924942	7.528193161	27.98632845	31.84778893	32.26081915
Staking fault	0.464850958	0.467477582	0.465223769	0.468159456	0.467024478

3.2. FTIR

The FTIR confirms the formation of hexagonal phases of different compositions. FT-IR spectra of $BaLa_xFe_{12-x}O_{19}$ (x=0.0, 0.25, 0.50, 0.75, and 1.00) with various La^{+3} ion compositions (x=0.0, 0.25, 0.50, 0.75, and 1). There are two frequency bands widths are tracked. From Fig 2 the two frequency bands are ranged as υ_2 =413 cm^{-1} and υ_1 =525-537cm^{-1}.υ_1 the large frequency (almost 510 -550) cm^{-1} due to the inherent absorption bands at the tetrahedral site, and the other is at low frequency range υ_2 (390-430) cm^{-1} due to octahedral extending bands (Sheikh et al., 2019). All of the characteristic peaks in Fig 2 can be attributed to M-type barium hexa ferrite. The values of υ_1 change to a higher wave number as the La^{3+} ion content rises, and this can be assigned to the M-type barium ferrite. The values of υ_1 change to a greater wavelength as the La^{3+} ion level increased, and this can be explained by two main realities. The first is that La^{+3} ions have a lower atomic weight than Fe^{3+} ions, and the second is that even the atomic weight is inversely proportional to the wave number (El-Sayed, Meaz, Amer, & El Shersaby, 2013). The gap in bond length of $Fe^{3+} - O^{-2}$ at tetrahedral and octahedral sites induced a shift in the intensity of the absorption bands, i.e. 'υ_1' and 'υ_2'. All of the prepared nanoparticle sets reveal that as the lanthanum concentration increased, the frequency band changes significantly, which may be attributed to grain size and lattice parameters (Shahzadi et al., 2020). Furthermore, Using the bandwidth knowledge, the force coefficients K_t and K_o for octahedral and tetrahedral locales are calculated using the formula below.

$$K_o = 0.942128M (\upsilon_2)^2/ (M+32) \tag{10}$$
$$K_t = \sqrt{2}K_o \upsilon_1/ \upsilon_2 \tag{11}$$

Where M shows the atomic weight of material, where υ_1 and υ_2 are different frequency. we investigate the constant force to improve the fixation, which demonstrates the conceivable reinforcing of bonding between.
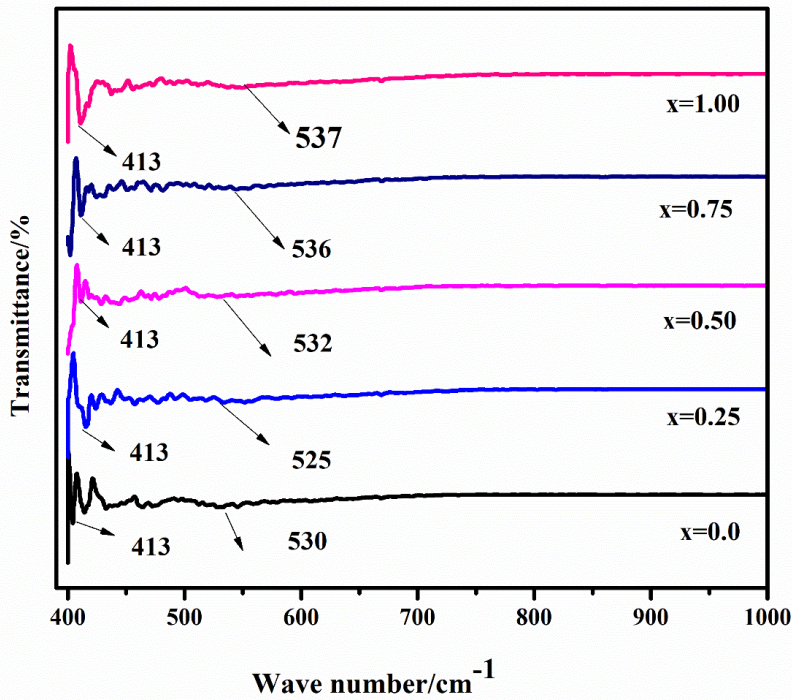
Figure 2: FTIR Spectra of $BaLa_xF_{12-x}O_{19}$

The tetrahedral and octahedral radii are likewise gotten from the accompanying equations.

$$R_{Tetra} = a\sqrt{3}(u-0.25) - R_o \qquad (12)$$
$$R_{octa} = a(5/8-u) - R_o \qquad (13)$$

Where R_{tetra} (tetrahedral radii) and R_{octa} (octahedral radii), also u and "a" are different parameter, in above equation "a" is known as lattice parameter and oxygen position parameter is u (Sheikh et al., 2019).

Table 3
The measured parameters for FTIR

Parameters	x = 0.0	x = 0.25	x = 0.50	x = 0.75	x = 1.00
Molecular weight	1111.47	1132.2363	1153.0025	1173.7688	1194.535
υ_1 / cm^{-1}	530	525	532	536	537
υ_2 / cm^{-1}	413	413	413	413	413
$K_o(dyne/cm^2) \times 10^5$	1.56201	1.56281	1.56358	1.56433	1.56505
$K_t/(dyne/cm^2) \times 10^5$	2.83481	2.80951	2.84838	2.87117	2.87785

3.3. Dielectric Properties

The dielectric properties of synthesized ferrite materials with a basic equation of $BaLa_xFe_{12-x}O_{19}$ (x = 0.0, 0.25, 0.50, 0.75, and 1.00) are measured at room temperature using LCR meter over a frequency range of 1 MHz to 3 GHz. Dielectric properties of M-type hexa-ferrites for the substitution of rare earth metal are studied as the function of frequency at encompassing temperature.

3.3.1. Dielectric Constant and Dielectric Loss

The graph between permittivity vs frequency is shown below. The dielectric constant has been measured experimentally by using formula given below.

$$\varepsilon' = C \times d / A \times \varepsilon \qquad (14)$$

Figures 3 display the variance of dielectric constant vs frequency for $BaLa_xFe_{12-x}O_{19}$ ferrites (x = 0.00, 0.25, 0.50, 0.75, 1.00) at room temperature. The statistics demonstrate that as the Fig 2 display the variance of dielectric constant, dielectric loss vs frequency for $BaLa_xFe_{12-x}O_{19}$ ferrites (x = 0.00, 0.25, 0.50, 0.75, 1.00) at room temperature. This were discovered that the electrical interchange among Fe^{2+} and Fe^{3+} causes neighborhood movement, which determine polarization. The plots demonstrate that equally real and imaginary components of dielectric constants indicate frequency scattering. The dielectric constant, dielectric loss values are low at low frequency but instead quickly increases as frequency increases along with frequency of whole structures, indicating a basic pattern for every ferrite sample, this action reflects dispersion. According to Koop's phenomenological theory, this behavior portrays dispersion caused by Maxwell Wagner type interfacial polarization (Iqbal, Islam, Ali, Sadiq, & Ali, 2014).
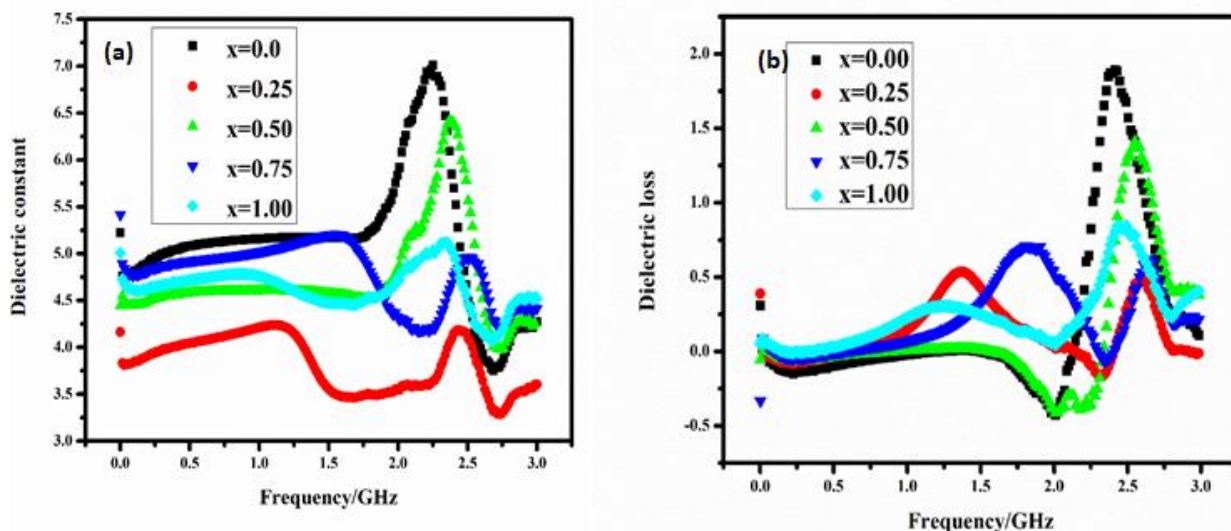
Figure 3: (a) The Dielectric Constant as a function Frequency (b) The Dielectric loss as function of Frequency

3.3.2. Tangent Loss and AC Conductivity

The graph clearly shows the tan loss goes down with growing frequency. The electrons follow the field when the frequency of the given alternating current of field of force is even lower compare the hopping frequency of ions among Fe^{2+} and Fe^{3+} electrons at neighboring octahedral sites, the ions obey the area thus loss was greatest. (Tan loss) is high at high frequency and rapidly increase at high frequency, according to Koop's phenomenological theorem. As a result, tan loss in the low frequency region is expected to be high, while tan loss in the high frequency region is expected to be high (Iqbal et al., 2014).

Table 4
Dielectric parameters for $BaLa_xFe_{12-x}O_{19}$

Parameters	Frequency	x = 0.0	x = 0.25	x = 0.50	x = 0.75	x = 1.00
Dielectric constant	1MHz	5.22376	4.16556	4.44576	5.41444	5.0067
	1GHz	5.159	4.21558	4.60433	5.02073	4.75967
	2.5GHz	4.49196	4.09188	5.56372	4.94024	4.45486
	3GHZ	4.27519	3.60566	4.25219	4.41541	4.52102
Dielectric loss	1MHz	0.30928	0.38993	-0.05495	-0.33232	0.0531
	1GHz	-0.02137	0.14784	0.00664	0.07233	0.22985
	2.5GHz	1.57008	0.3185	1.31588	0.23878	0.8102
	3GHZ	0.1106	-0.01209	0.38168	0.21544	0.40735
Tan loss	1MHz	0.05921	0.09361	-0.01236	-0.06138	0.01061
	1GHz	-0.00414	0.03507	0.00144	0.01441	0.04829
	2.5GHz	0.34953	0.07784	0.23651	0.04833	0.18187
	3GHZ	0.02951	0.00163	0.09316	0.05468	0.09635

About 1 MHz and 3 GHz, the AC conductivity of the prepared ferrite sample $BaLa_xFe_{12-x}O_{19}$ (x = 0.0, 0.25, 0.50, 0.75, 1.00) is measured. The expression to be utilized

$$\sigma_{ac} = (t / A) \times [z'/(z'^2 + z''^2)] \tag{15}$$

where "*t*" shows that the thickness of pellet, area of the pellet is known as A, Fig 5 illustrates the frequency-dependent alternating current conductivity of all sintered material. The AC conductivity with all samples start to increases from low frequency range, but dispersion conducting was observed at higher frequencies. Ferrite substance are made up of transmitting grains isolated by conductive small sections of grain borders, according to both the Maxwell–Wagner model and the Koop's conceptual principle. Since dielectric distortion is related to absorption processes. Because of growing resistance of crystal structure the activity of all composition seems to be the same at low frequency (Parveen et al., 2019).
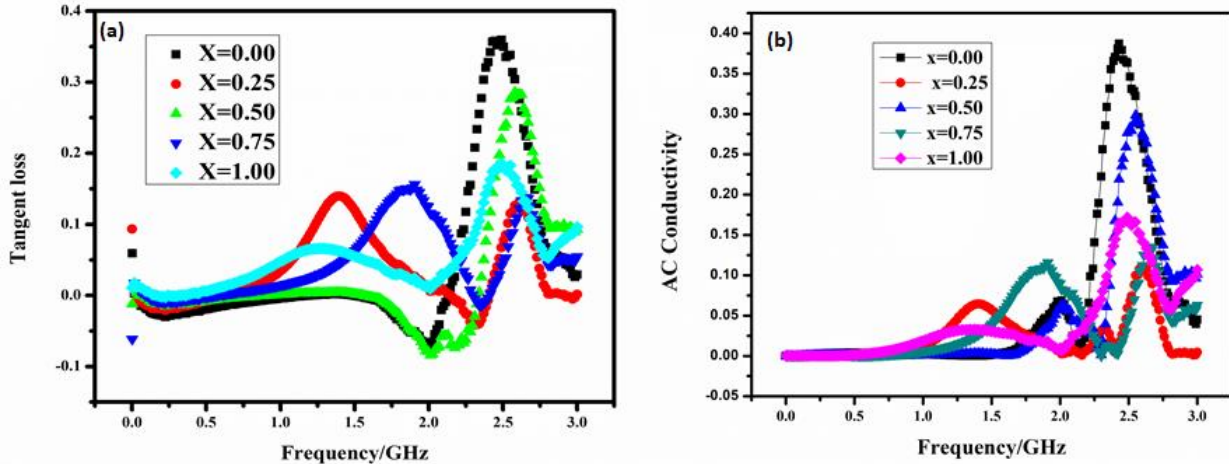
Figure 4: (a) Tangent loss as a function of frequency (b) AC conductivity as a function of frequency

3.3.3.Real and Imaginary Impedance

Impedance is important in deciding the dielectric possessions of materials. The real and imaginary impedances are strongly directly proportional to the frequency. Fig 6 represent the impedance as a role of the frequency, which ranges between 1 MHz and 3 GHz. The real and imaginary impedance portions of impedance are measured as for each ferrite $BaLa_xFe_{12-x}O_{19}$ (x = 0.0, 0.25, 0.50, 0.75, 1.00),. By using the following formula to calculate the real and imaginary impedance.

$$Z' = R = |Z| \cos \theta_z, \tag{16}$$
$$Z'' = X = |Z| \sin \theta_z, \tag{17}$$

According to impedance analysis, the rise of The frequency at which it is used eliminates the real and imaginary sections of impedance. The impedance plot changes as when the frequency increases, the all the specimens converge on one another, and at a higher frequency, the impedance exhibits coherent nature, which is due to the discharge of space charges. The decrease in real and imaginary impedance components means that conductivity improves as field frequency increases, owing to the concentration difference and the non-uniformity of the given field, which tends to add these distinct charges on the crystal structure. Above are both the imaginary and real impedance diagram.
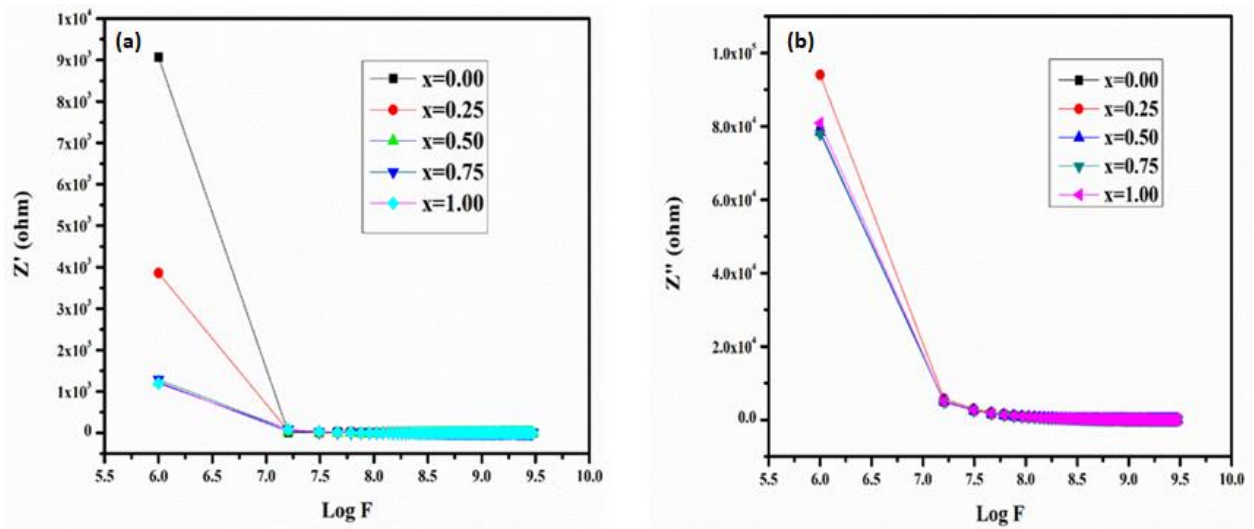
Figure 6: (a) The Real impedance as a function with log of frequency (b) The Imaginary impedance as function with log of frequency

3.3.4. Real and Imaginary Electric Modulus

Modulus structures were being utilized to investigate the position of grain boundaries over a defined frequency spectrum. Under the given frequency, the imaginary and real modulus of samples is investigated. The following are the formulas for calculating real and imaginary modulus.

$$M^{'} = \varepsilon^{'}/(\varepsilon^{'2}+\varepsilon^{''}) \qquad (18)$$
$$M^{'''} = \varepsilon^{''}/(\varepsilon^{'2}+\varepsilon^{''}) \qquad (19)$$

Figures 7 demonstrate the real and imaginary electric modulus. At short frequencies, the real and imaginary components of the electric modulus have very small rates and rise sequentially as the given field frequency rises, while at large frequencies, they reach their limit (3 GHz) (Parveen et al., 2019).The electrical modulus of $BaLa_xFe_{12-x}O_{19}$ ferrites, which induced electrically charged concentration across the inorganic nanoparticles in expelling stimulation peaks, is used to investigate the frequency response of the concentration polarization impact. The sample of impedance with Z" vs Z' provides a better representation of the concentric spheres in the plane if the region of accuracy of the grain boundary is reduced. If the crystal structure region covers a great volume, the trend for modulus M" vs M' provides huge data about the semicircle.
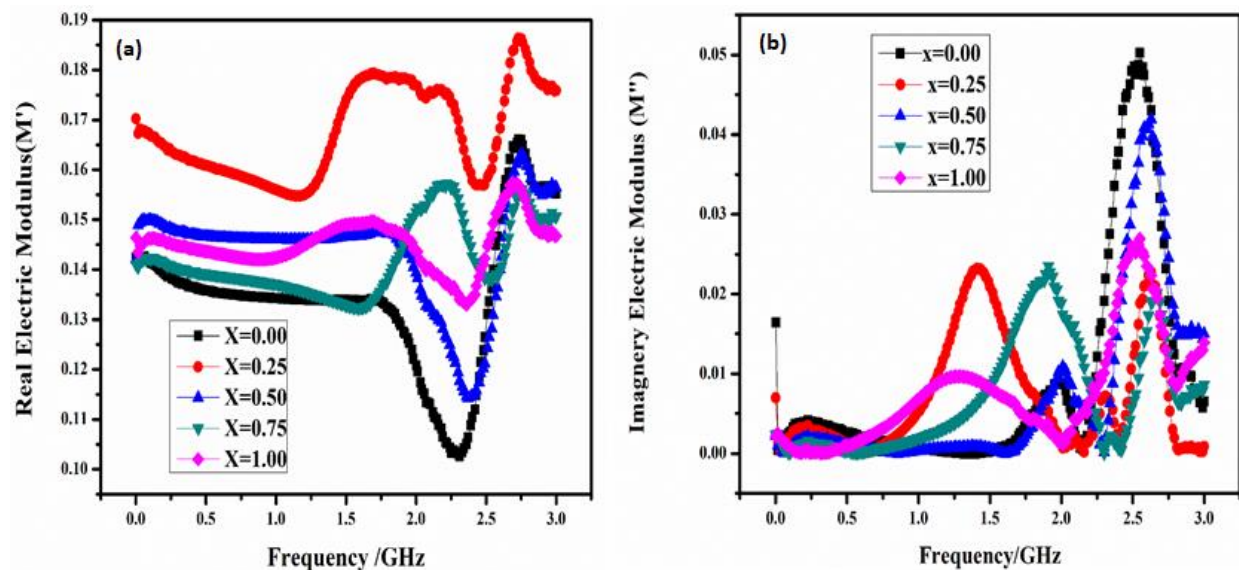
Figure 7: (a) Real Electric Modulus as a function of Frequency (b) Imaginary Electric Modulus as a function of Frequency

Table 5
AC conductivity, Impedance, Modulus for $BaLa_xFe_{12-x}O_{19}$ (X=0.00, 0.25, 0.50, 0.75, 1.00)

Parameters	Frequency	X=0.00	X=0.25	X=0.50	X=0.75	X=1.00
AC conductivity	1 MHZ	4.4444E-05	1.336E-05	6.119E-06	6.5352E-06	5.62068E-06
	1 GHZ	0.00221902	0.0123562	0.000939	0.00582268	0.019071805
	2.5 GHZ	0.34628092	0.0683428	0.282689	0.0482143	0.16648189
Z' (ohms)	1 MHZ	82209147.0	14892846	1504486.	1666936.62	1430707.84
	1 GHZ	0.15416373	8.7130111	0.038683	1.15298201	14.4860242
	2.5 GHZ	114.489572	7.4630427	55.06665	2.15162838	32.3932633
z"(ohms)	1 MHZ	618646744	88370979	61590350	606886338	653764098
	1 GHZ	5436.83400	7331.8375	6432.649	5665.38172	6117.66131
	2.5 GHZ	834.987484	1221.1404	751.5586	932.680606	1018.09238
M'	1 MHZ	0.1424188	0.1702161	0.1421027	0.1410586	0.1464052
	1 GHZ	0.1342679	0.1559214	0.1460475	0.137061	0.1424269
	2.5 GHZ	0.1310757	0.1585131	0.1243551	0.1385316	0.1447358
M"	1 MHZ	0.0164175	0.0069877	0.002221	0.0023378	0.00216581
	1 GHZ	0.000715	0.0053751	0.0003581	0.0019553	0.00693064
	2.5 GHZ	0.0485361	0.012392	0.033661	0.0066537	0.02581722

4. Conclusion

From decades, these ferrites were regarded as extremely useful electrical materials. The ferrite compounds have a hexagonal structure, but there is also a category of ferrites called hexaferrites that have a hexagonal crystal structure. Nano structural and dielectric features for $BaFe_{12-x}La_xO_{19}$ (0.00, 0.25.0.50, 0.75, 1.00) nano Hexaferrite (NHFs) was studied present research. The Ba NHF prepared via sol-gel technique. The sol gel process is used to efficiently synthesize Nano crystalline ferrite with the structural formula $BaLa_xFe_{12-x}O_{19}$ (x=0.00, 0.25, 0.50, 0.75, 1.00).sol gel technique is very easy method to synthesized that type of ferrite. With their sharp peak, XRD studies affirm the hexagonal structure. The Debye Scherer expression is used to measure crystalline size, which is observed to be in the Nano size range of 13 nm to 5 nm. The lattice constant also calculated by using the hkl with respect to the present materials JCPDS Card. The values of the lattice constant "a" in range from 5.83 Å to 5.90 Å, as with different concentrations, it gives different rising and decreasing patterns. The values of the lattice constant "c" in range from 23.10 Å to 23.83 Å, as with different concentrations, it gives different rising and decreasing patterns due to ionic radii. The crystal size pattern shows the decreasing order in crystal size. The FTIR confirms the formation of hexagonal phases of different compositions. FTIR findings indicate two stretching frequency bands corresponding to octahedral and tetrahedral, which are typical bands of hexagonal ferrite. In the frequency range of 1 MHZ to 3GHZ. The two frequency $υ_2$ =413 cm^{-1} and the other $υ_1$ =525-537cm^{-1}. $υ_1$ is the large frequency (almost 510 -550) cm^{-1} due to the inherent absorption bands at the tetrahedral site, and the other is at low frequency range $υ_2$ (390-430) cm^{-1} due to octahedral extending bands. Dielectric experiments are carried out. Dielectric experiments give the permittivity and permit loss increase as change with frequency. The real and imaginary impedance curves change as when the frequency increases, the all the specimens converge on one another, and at a higher frequency, the impedance exhibits coherent nature, which is due to the discharge of space charges. There are many others parameters are calculated in dielectric properties such as real and imaginary electric modulus, real and imaginary impedance, dielectric constant, dielectric loss and tangent loss.

Conflict of Interest

The authors declare that they have no conflict of interest.

Reference

Al-Hilli, M. F., Li, S., & Kassim, K. S. (2012). Structural analysis, magnetic and electrical properties of samarium substituted lithium–nickel mixed ferrites. *Journal of Magnetism and Magnetic Materials, 324*(5), 873-879.

Azim, M., Atiq, S., Riaz, S., & Naseem, S. (2014). *Indexing the structural parameters and investigating the magnetic properties of lanthanum doped strontium hexaferrites.* Paper presented at the IOP Conference Series: Materials Science and Engineering.

Carter, C. B., & Norton, M. G. (2007). *Ceramic materials: science and engineering* (Vol. 716): Springer.

Cullity, B. D. (1978). Elements of X-ray diffraction, Addison. *Wesley Mass*.

El-Sayed, S., Meaz, T., Amer, M., & El Shersaby, H. (2013). Magnetic behavior and dielectric properties of aluminum substituted M-type barium hexaferrite. *Physica B: Condensed Matter, 426*, 137-143.

Garcia, R. M., Bilovol, V., & Socolovsky, L. (2012). Effect of the heat treatment conditions on the synthesis of Sr-hexaferrite. *Physica B: Condensed Matter, 407*(16), 3109-3112.

Gilani, Z. A., Warsi, M. F., Khan, M. A., Shakir, I., Shahid, M., & Anjum, M. N. (2015). Impacts of neodymium on structural, spectral and dielectric properties of LiNi0. 5Fe2O4 nanocrystalline ferrites fabricated via micro-emulsion technique. *Physica E: Low-dimensional Systems and Nanostructures, 73*, 169-174.

Hussain, S., & Maqsood, A. (2008). Structural and electrical properties of Pb-doped Sr-hexa ferrites. *Journal of Alloys and Compounds, 466*(1-2), 293-298.

Hussain, S., Shah, N. A., Maqsood, A., Ali, A., Naeem, M., & Syed, W. A. A. (2011). Characterization of Pb-doped Sr-ferrites at room temperature. *Journal of superconductivity and novel magnetism, 24*(4), 1245-1248.

Iqbal, M. A., Islam, M., Ali, I., Sadiq, I., & Ali, I. (2014). High frequency dielectric properties of Eu+ 3-substituted Li–Mg ferrites synthesized by sol–gel auto-combustion method. *Journal of Alloys and Compounds, 586*, 404-410. doi:10.1016/j.jallcom.2013.10.066

Onreabroy, W., Papato, K., Rujijanagul, G., Pengpat, K., & Tunkasiri, T. (2012). Study of strontium ferrites substituted by lanthanum on the structural and magnetic properties. *Ceramics International, 38*, S415-S419.

Parveen, A., Khalid, M., Gilani, Z. A., Aslam, S., Saleem, M., Shaikh, F. A., & Rehman, J. (2019). Dielectric, impedance and modulus spectroscopic studies of Co 0.3 Cd 0.7 Zn 1.5 x Fe 2− x O 4 nanoparticles. *Applied Physics A, 125*(10), 1-11.

Shahzadi, K., Chandio, A. D., Mustafa, G., Khalid, M., Khan, J. K., Akhtar, M. S., & Gilani, Z. A. (2020). Impact of aluminum substitution on the structural and dielectric properties of Ni–Cu spinel ferrite nanoparticles synthesized via sol–gel route. *Optical and Quantum Electronics, 52*(4), 1-17.

Sheikh, F. A., Khalid, M., Shifa, M. S., Aslam, S., Perveen, A., ur Rehman, J., . . . Gilani, Z. A. (2019). Effects of bismuth on structural and dielectric properties of cobalt-cadmium spinel ferrites fabricated via micro-emulsion route. *Chinese Physics B, 28*(8), 088701.

Smit, J., & Wijn, H. (1959). Ferrites, philips technical library. *Eindhoven, The Netherlands, 278*.